Typical synoptic situations and their impacts on the wintertime air pollution in the Guanzhong basin, China

N. Bei[1,2*], G. Li[2,3*], R. Huang[2,4], J. Cao[2,3], N. Meng[1], T. Feng, S. Liu[2,3], T. Zhang[2,3], Q. Zhang[5], and L. T. Molina[6]

(1) School of Human Settlements and Civil Engineering, Xi'an Jiaotong University, Xi'an, China
(2) Key Laboratory of Aerosol Chemistry and Physics, Institute of Earth Environment, Chinese Academy of Sciences, Xi'an, China
(3) State Key Laboratory of Loess and Quaternary Geology, Institute of Earth Environment, Chinese Academy of Sciences, Xi'an, China
(4) Laboratory of Atmospheric Chemistry, Paul Scherrer Institute (PSI), 5232 Villigen, Switzerland
(5) Department of Environmental Sciences and Engineering, Tsinghua University, Beijing, China
(6) Molina Center for the Energy and the Environment, La Jolla, CA, USA

Abstract: Rapid industrialization and urbanization have caused severe air pollution in the Guanzhong basin, northwestern China with heavy haze events occurring frequently in recent winters. Using the NCEP reanalysis data, the large scale synoptic situations influencing the Guanzhong basin during wintertime of 2013 are categorized into six types to evaluate the contribution of synoptic situations to the air pollution, including "north-low", "southwest-trough", "southeast-high", "transition", "southeast-trough", and "inland-high". The FLEXPART model has been utilized to demonstrate the corresponding pollutant transport patterns for the typical synoptic situations in the basin. Except "southwest-trough" and "southeast-high" (defined as favorable synoptic situations), the rest four synoptic conditions (defined as unfavorable synoptic situations) generally facilitate the accumulation of air pollutants, causing heavy air pollution in the basin. In association with the measurement of $PM_{2.5}$ (particulate matter with aerodynamic diameter less than 2.5 μm) in the basin, the unfavorable synoptic situations correspond to high $PM_{2.5}$ mass concentrations or poor air quality and vice versa. The same analysis has also been applied to winters of 2008-2012, which shows that the basin was mainly influenced by the unfavorable synoptic situations during wintertime leading to poor air quality. The WRF-CHEM model has further been applied to simulate the selected six days representing the typical synoptic situations during the wintertime of 2013, and the results generally show a good consistence between the modeled distributions and variations of $PM_{2.5}$ and the corresponding synoptic situations, demonstrating reasonable classification for the synoptic situations in the basin. Detailed meteorological conditions, such as temperature inversion, low-level horizontal wind speed, vertical wind velocity, and convergence all contribute to heavy air pollution events in the

* Correspondence to: Naifang Bei (bei.naifang@mail.xjtu.edu.cn) and Guohui Li (ligh@ieecas.cn)

basin under unfavorable synoptic conditions. Considering the proportion of occurrence of unfavorable synoptic situations during wintertime, reduction of emissions is the optimum approach to mitigate the air pollution in the Guanzhong basin.

Key words: synoptic situations, air pollution, Guanzhong basin

1. Introduction

Elevated atmospheric pollutants, such as particulate matter (PM) and ozone (O_3), exert deleterious impacts on human health and environment (e.g., Penner et al., 2001; Pope and Dockery, 2006; Zhang et al. 2010). Over the past three decades, with tremendous economic growth in China, rapid industrialization and urbanization have caused severe air pollution, as reflected in the heavy haze event that often occurs in the north of China, particularly during wintertime (e.g., Chan and Yao, 2008; Fang et al., 2009; Gao et al., 2011; Liu et al., 2013; Zhao et al., 2013; Huang et al., 2014; Fu et al., 2014; Guo et al. 2014; Han et al. 2014; Zhang et al., 2015; Yang et al. 2015). Guanzhong basin is located in the northwest of China, nestled between the Qinling Mountains in the south and the Loess Plateau in the north. The unique topography facilitates the accumulation of air pollutants, and with the rapid increasing industries and city expansions, heavy air pollution frequently attacks the basin (e.g., Cao et al, 2009; Sheng et al., 2011).

Numerous studies have demonstrated that the meteorological conditions play an important role in the formation, transformation, diffusion, transport, and removal of the atmospheric pollutants (e.g., Seaman, 2000; Solomon et al., 2000; de Foy et al., 2005, 2006; Bei et al., 2008, 2010, 2012, 2013). If the emissions of pollutants remain invariable, transformations in the chemical state of the atmosphere are principally determined by the meteorological conditions. Recent advances in understanding the role of the meteorological conditions in the air pollution formation in China have mainly concentrated on the regions of Beijing-Tianjin-Hebei, the Pearl River Delta, and the Yangtze River Delta (e.g., Wu et al., 2008, 2013; Wang et al., 2009; Zhang et al., 2010; Gao et al., 2011; Zhang et al., 2012; Wang et al. 2014a; Wang et al. 2014b; Zhang et al. 2015). Wang et al. (2009) have shown that the O_3 decrease at a Beijing rural site during the 2008 Olympics is attributed to the favorable meteorological condition in comparison with the same period in 2006 and 2007. Zhang et al.

(2010) have proposed that, during the 2008 Olympics, the atmospheric visibility improvements are likely caused by the decrease of atmospheric relative humidity compared to the same period in the previous 5 years. Using a coupled meteorology-chemistry model, Gao et al. (2011) have further pointed out that meteorological conditions are as important as emission controls in reducing aerosol concentrations in Beijing during the 2008 Olympics. Wu et al. (2008) have performed analysis of the typical haze and clean weather processes over the Pearl River Delta in 2004 and 2005, and found that the regional haze formation is highly correlated to the regional calm wind process while the cleaning process is influenced by the strong advection transport. Additionally, Wu et al. (2013) have classified two typical weather conditions associated with poor air quality over the Pearl River Delta, including the warm period before a cold front and the subsidence period controlled by a tropical cyclone during two intensive observations in 2004 and 2006. Wang et al. (2014b) have demonstrated that recirculation and regional transport, along with the poorest diffusion conditions and high humidity favorable for hygroscopic growth of secondary aerosols, caused the extremely high levels of $PM_{2.5}$ in Beijing during January 2013. Zhang et al. (2015) have also suggested that the weak transport/diffusion was an important factor for the haze occurrences.

The circulation-based classification is an approach to identify synoptic weather categories through determining the circulation types from sea level pressure, geopotential height, or wind fields (Huth et al., 2008). Since the meteorological fields that affect the air quality are generally closely interrelated and strongly controlled by the synoptic-scale circulation, the circulation classification has been extensively used in environmental studies, especially in the middle and high latitude regions where local weather conditions are chiefly determined by the day-to-day synoptic circulation variability (e.g., Jacobeit, 2010; Huth et al., 2008). For example, Bei et al. (2013) have classified the typical synoptic situations and the associated plume transport patterns in the US-Mexico border region along the Pacific Ocean,

and found that the plume transport directions are generally consistent with the prevailing wind directions on 850 hPa. However, only a few studies have been performed to investigate the synoptic weather classification in China (Huth et al., 2008). Cheng et al. (2001) have demonstrated that high O_3 concentrations at Taiwan are related to anticyclonic synoptic systems and a tropical low-pressure system moving from the south of Taiwan. Recent studies have also indicated that the developing and different parts of an anticyclonic system play an important role in regulating air quality (Chen et al., 2008; Wei et al., 2011). However, the above-mentioned studies are all based on case studies during a short period using subjective procedure. Zhang et al. (2012) have verified the relationship between surface circulation pattern and air quality in Beijing and the surrounding areas over 10 years using a synoptic approach based on an objective classification procedure (Philipp et al. 2010). Results have demonstrated that significant differences exist in the local meteorology and footprints of 48-h backward trajectories among various circulation types, and synoptic-scale circulations are the principal drivers of day-to-day variations in pollutant concentrations over Beijing and surrounding areas during the emission control period.

Previous studies have examined the composition, characteristics, and sources of the atmospheric pollutants in the Guanzhong basin (e.g. Cao et al. 2009; 2012; Shen et al. 2010; 2011). However, few studies have been performed to comprehensively explore the relationship between air pollution and the meteorological conditions at both synoptic and local scales in this area. Therefore, it is imperative to examine the role of the specific meteorological conditions in the formation of heavy air pollution in this area to support design and implementation of emission control strategies.

The purpose of the present study was to categorize the large-scale synoptic weather systems that impact the Guanzhong basin in the winter along with the measurements of pollutants in the basin using a subjective classification procedure, which determines the

124 circulation types from the geopotential height and wind fields on 850 hPa. The air quality
125 situations associated with various synoptic situations are simulated using the WRF-CHEM
126 model developed by Li et al. (2010; 2011a; 2011b), to evaluate the contributions of the
127 particular meteorological conditions to the severe air pollution. The models and methodology
128 used in this study are introduced in Section 2. The main results are presented in Section 3.
129 Conclusions and discussions are given in Section 4.
130

131 **2. Data, Models, and Methodology**

132 The National Centers for Environmental Prediction (NCEP) final operational global
133 gridded analysis (FNL) (1°×1°) is used to categorize the large-scale synoptic weather systems
134 influencing the Gunazhong basin during the period from 2008 to 2013 through the subjective
135 procedure. The geopotential height and wind fields on 850 hPa are applied to identify the
136 synoptic situations that affect the plume transport patterns in the basin.

137 Continuous daily $PM_{2.5}$ measurements have been performed at the Institute of Earth
138 Environment, Chinese Academy of Sciences (IEECAS) in Xi'an, China since 2003.
139 Additionally, since January 2013, the China's Ministry of Environmental Protection (China
140 MEP) has commenced to release the real-time hourly concentrations of $PM_{2.5}$. Total 33
141 monitoring sites are distributed in the Guanzhong basin (Figure 1b). The daily $PM_{2.5}$
142 measurement at IEECAS site from 2008 to 2012 and the hourly $PM_{2.5}$ measurement released
143 by China MEP from 2013 to 2014 are used to validate the categorized synoptic situations
144 influencing the basin.

145 In order to analyze the corresponding pollutant transport patterns under the typical
146 categorized synoptic situations, The FLEXPART model is employed to calculate the forward
147 Lagrangian particle dispersion (Stohl et al., 1998; Fast and Easter, 2006), which is driven by
148 the output from the WRF model (Skamarock et al. 2008). The FLEXPART model is set-up

149 with releases of 6,000 computational particles within a grid cell of 10 km × 10 km × 0.02 km
150 centered at Xi'An urban area in the morning. Tracer particles are released continuously from
151 04:00 to 10:00 BJT (Beijing Time) of the day, and traced until 04:00 BJT of next day. For the
152 convenience, all the time used hereafter is BJT. The WRF model adopts one grid with
153 horizontal resolution of 3-km and 35 sigma levels in the vertical direction. The grid cells used
154 for the domain are 201×201 (Figure 1a). The selected six days, representing six categorized
155 typical synoptic situations of the Guanzhong basin during wintertime of 2013, are simulated.
156 They are initialized at 20:00 BJT on each day and integrated for 36 hours. The NCEP FNL
157 analysis data (1°×1°) is used to produce the initial and boundary conditions for the WRF
158 model. The physical process parameterization schemes used in simulations included the
159 Grell-Devenyi ensemble scheme for cumulus scheme (Grell and Devenyi, 2002), the WRF
160 Single Moment (WSM) three-class microphysics (Hong et al., 2004), and Mellor-Yamada-
161 Janjic (MYJ) TKE scheme (Janjic, 2002) for the PBL processes.
162 The WRF-CHEM model has been used to further simulate the selected six days
163 representing the typical categorized synoptic situations and to verify the particular
164 meteorological conditions during the severe air pollution events in the Guanzhong basin. A
165 specific version of the WRF-CHEM model (Grell et al., 2005) is used in the present study,
166 which was developed by Li et al. (2010; 2011a, b; 2012) at the Molina Center for Energy and
167 the Environment, with a new flexible gas phase chemical module and the CMAQ (version 4.6)
168 aerosol module developed by US EPA (Binkowski and Roselle, 2003). The inorganic
169 aerosols are simulated in the WRF-CHEM model using ISORROPIA ("equilibrium" in Greek,
170 here referred to as an improved thermodynamic equilibrium aerosol model) Version 1.7
171 (http://nenes.eas.gatech.edu/ISORROPIA/). The secondary organic aerosols (SOA) formation
172 is simulated using a non-traditional SOA model including the volatility basis-set modeling
173 method in which primary organic components are assumed to be semi-volatile and

174 photochemically reactive and are distributed in logarithmically spaced volatility bins (Li et al.,
175 2011a). Detailed description of the WRF-CHEM model can be found in Li et al. (2010;
176 2011a, b; 2012). The meteorological setup in the WRF-CHEM model simulations is same as
177 those in the WRF model, except that the spin-up time of the WRF-CHEM model is one day.
178 The chemical initial and boundary conditions for the WRF-CHEM model simulations are
179 interpolated from the 6-h output of a global chemical transport model for O_3 and related
180 chemical tracers (MOZART). The anthropogenic emission inventory (EI) developed by
181 Zhang et al. (2009) is used in the study, including contributions from agriculture, industry,
182 power, residential and transportation sources. The MEGAN model developed by Guenther et
183 al. (2006) is used to calculate on-line biogenic emissions.
184
185 **3. Results**
186 NCEP-FNL reanalysis data, the model output from the FLEXPART model, and the
187 $PM_{2.5}$ measurements in the Guanzhong basin are used to explore the typical meteorological
188 synoptic situations and the corresponding plume transport patterns. Using the model output
189 from the WRF-CHEM model, we have further investigated the local meteorological
190 conditions, including the PBL height, low level wind speed, inversion layer, low level
191 convergence and divergence, and vertical wind velocity, and their potential impacts on the air
192 pollution formation process in the basin.
193 **3.1 Classification of the Typical Synoptic Situations and the Corresponding Pollutant**
194 **Transport Patterns**
195 Based on the NCEP-FNL reanalysis data, we have first performed the analysis of the
196 synoptic situations during the wintertime of 2013 using the 850 hPa wind and geopotential
197 height fields. Here the wintertime is defined as December of the year to February of the next
198 year. Six typical synoptic situations are categorized, including “north-low”, “southwest-

trough", "southeast-high", "transition", and "inland-high". The detail dates are shown in table 1. The percentages of the above-mentioned six types are 17.8%, 14.4%, 4.4%, 12.2%, 5.6%, and 45.6%, respectively, indicating that the "inland-high" is the dominant wintertime synoptic situation influencing the Guanzhong basin.

Figure 2 shows 850 hPa winds and geopotential heights at 08:00 BJT for the selected 6 days representing the six categorized typical synoptic situations, respectively, including (1) Feb. 16, 2014 ("north-low"), (2) Jan. 19, 2014 ("southwest-trough"), (3) Dec. 26, 2013 ("southeast-high"), (4) Dec. 2, 2013 ("transition"), (5) Jan. 23, 2014 ("southeast-trough"), and (6) Dec. 23, 2013 ("inland-high"). In case of the "north-low" (Figure 2a), the Guanzhong basin is generally located in the north of the low on 850 hPa and the weak east wind is prevalent aloft. Due to the blocking of the specific topography (Figure 1a), the convergence or stagnant conditions are frequently formed, which is not favorable for the dispersion of air pollutants. However, heavy air pollution might not emerge in the basin due to the occurrence of precipitation, which is caused by the favorable dynamical conditions that can efficiently clean up the pollutants. For the category of "southwest-trough" (Figure 2b), the basin is located in the southwest of the trough on 850 hPa and the northwest wind is prevailing over the basin. The cold and dry air from the northwest effectively evacuates the air pollutants formed in the basin and also brings blue sky for the basin. For the category of "southeast-high" (Figure 2c), the high of 850 hPa in the northwest of the basin originates the prevalent northeasterly or northwesterly winds, transporting the pollutants outside of the basin and remarkably improve the air quality. When the basin is situated in the transition area between the trough in the north and the high in the south on 850 hPa, the synoptic situation is defined as the category of "transition" (Figure 2d). The prevailing winds over the basin are generally westerly, but the west wind is significantly attenuated by the topography in the basin and often transformed to be calm or disordered. The atmospheric pollutants are subject to be

conveyed to the east of the basin, but more likely to be trapped in the basin, causing heavy air pollutions. Additionally, in the condition of "transition", the meteorological fields in the basin are also coordinately adjusted with the development of the trough in the north and the high in the south on 850 hPa. Under the condition of "southeast-trough" (Figure 2e), the basin is affected by the trough on 850 hPa in the northwest, and the southwest wind is dominant aloft. The weak south winds and convergence formed in front of the trough tend to withhold the air pollutants in the basin, significantly deteriorating the air quality. For the category of "inland-high" (Figure 2f), the basin is controlled by the inland high on 850 hPa, and the prevailing wind is varied over the basin, depending on the detailed location of the high. The situation of weak winds, subsidence, and the stable stratification facilitates the accumulation of atmospheric pollutants, often causing severe air pollutions in the basin.

Figure 3 displays the 24-hour plume transport patterns initialized from 04:00 BJT on the abovementioned 6 representative days. The particles released in the morning in the urban area of Xi'an are generally transported within the planetary boundary layer (PBL). Apparently, only in case of "southwest-trough" and "southeast-high", the particles can be transported outside of the basin and the improvement of air quality in the basin is anticipated. For the rest four synoptic categories, most of released particles ramble in the basin, indicating buildup of the air pollutants.

The above analyses demonstrate that only two kinds of synoptic conditions ("southwest-trough" and "southeast-high", defined as favorable synoptic situations hereafter) disperse pollutants efficiently and engender the good air quality in the Guanzhong basin. The rest four kinds of synoptic situations ("north-low", "transition", "southeast-trough", and "inland-high", defined as unfavorable synoptic situations hereafter) are generally favorable for the accumulation of the air pollutants either in horizontal or vertical directions, except in case of the "north-low" with strong winds or precipitation or the "southeast-trough" with

249 strong vertical mixings.

250 Figure 4 displays the average diurnal cycle of observed $PM_{2.5}$ mass concentrations at
251 33 monitoring sites in the Guanzhong basin under the six synoptic categories during the
252 wintertime of 2013. Consistently, the favorable synoptic situations correspond to low $PM_{2.5}$
253 mass concentrations or relatively good air quality and vice versa. Under the unfavorable
254 synoptic situations, the observed average $PM_{2.5}$ mass concentrations generally range from
255 150 to 250 μg m^{-3}, showing that the basin has experienced heavy air pollution. The $PM_{2.5}$
256 mass concentrations in case of "north-low" are lower than those under the rest three
257 unfavorable synoptic situations, which is caused by the possible occurrence of precipitation
258 in the condition of "north-low". For example, the synoptic patterns on Feb. 4 and 5, 2014 are
259 categorized to "north-low", but the observed average $PM_{2.5}$ mass concentrations are less than
260 90 μg m^{-3} because of the precipitation washout on these two days. Although the favorable
261 synoptic situations facilitate the evacuation of air pollutants in the basin, the observed
262 average $PM_{2.5}$ mass concentrations still exceed 35 μg m^{-3}, indicating that the air quality in the
263 basin barely reaches the excellent level. It should be noted that the exceptional days exist
264 beyond the six synoptic situations, indicating the complexity of atmospheric circulations.

265 With the same method as used in 2013, we have further classified the large-scale
266 synoptic situations of the wintertime in the Guanzhong basin for the period from 2008 to
267 2012. The above-mentioned six typical synoptic situations influencing the Guanzhong basin
268 during the wintertime from 2008 to 2012 are summarized in Table 2. Figure 5 displays the
269 daily mean $PM_{2.5}$ mass concentration averaged during the six typical synoptic situations from
270 2008 to 2012 at the IEECAS site. The percentage of total unfavorable synoptic situations
271 during 2008 to 2012 is about 85%, and corresponding daily $PM_{2.5}$ mass concentrations
272 exceed 200 μg m^{-3} (Figure 5), indicating the significant contribution from the large-scale
273 meteorological conditions to the poor air quality in the basin. The "inland-high" dominates

the synoptic situation in association with the poor air quality in the basin, with the contribution of around 43%. The favorable situations constitute about 15% of the synoptic situation in the basin, which is anticipated to empty the basin and significantly improve the air quality. However, the observed daily $PM_{2.5}$ mass concentrations during the favorable situations still exceed 75 $\mu g\ m^{-3}$ and fail to reach the good level, indicating the massive local emissions of pollutants and considerable contributions of background dust transport from Loess plateau in the north.

3.2 Local Meteorological Conditions on the Selected 6 Days and Their Impact on the Air Quality

The results of the FLEXPART model only explain the direct impact of the meteorological fields on the plume transport process since chemical processes are not considered in the model. The WRF-CHEM model is therefore used to simulate the air quality in the Guanzhong basin on the selected six days corresponding to the above-mentioned six kinds of typical synoptic situations.

Figure 6 provides the vertical distributions of temperature, wind vectors, and PBL height through Xi'An along the east-west direction at 09:00 and 15:00 BJT on the selected six days, in order to investigate the vertical atmospheric characteristics under the six typical synoptic situations. The vertical section shows the depth of the basin is around 1 km, indicating that the local terrain (Loess Plateau and Qinling Mountains) has important impacts on the low-level wind fields inside the basin. Under unfavorable synoptic situations, the winds inside the basin are remarkably attenuated due to the influence of the terrain, favorable for trapping the air pollutants formed in the basin. In addition, at 09:00 BJT, temperature inversions in case of unfavorable synoptic situations also impede the development of PBL, decreasing the diffusion of air pollutants in the vertical direction. At 15:00 BJT, the weak winds do not boost the PBL development due to lack of the wind shear inside the basin and

299 the thermal impact dominates the PBL height. The PBL on Dec. 02, 2013 and Jan. 23, 2014
300 is higher than that on Feb. 16, 2014 and Dec. 23, 2013 due to the low-level temperature
301 discrepancy, and the impact of the urban heat island on the PBL height is also obvious.
302 Therefore, the unfavorable synoptic situations are prone to trap the pollutants inside the basin
303 due to inefficient horizontal transportation and impeded vertical diffusion, leading to the
304 heavy air pollution in the basin. In case of favorable synoptic situations, the strong horizontal
305 wind (Jan. 19, 2014) or active vertical motion (Dec. 26, 2013) efficiently diffuse the
306 pollutants in the horizontal or vertical directions and the high PBL also expedites the vertical
307 exchange of air pollutants in the basin, so the good air quality is expected.

308 To investigate the detailed local meteorological conditions over the Guanzhong basin
309 on the above-mentioned six days, we have further analyzed the low-level (below 850 hPa)
310 vertical motion, divergence, and horizontal wind speed averaged over the Guanzhong basin
311 (the averaged domain indicated in Figure 1). Figure 7 shows the time-evolutions of the area
312 averaged low-level vertical velocity, divergence, and wind speed over the basin on the
313 selected 6 days. In general, under favorable synoptic situations, the divergence exists in the
314 low-level atmosphere inside the basin, leading to the strong downward motion and
315 outflowing of pollutants from the basin. In addition, the occurrence of strong horizontal
316 winds also speeds up the evacuation of pollutants, such as on Jan. 19, 2014, the average wind
317 speed is around 8 m s^{-1}. Under the unfavorable conditions, except on Dec. 02, 2013, the weak
318 convergence leads to slow upward motions, which withholds the pollutants inside the basin,
319 and the weak horizontal winds also inefficiently disperse the pollutants, i.e., the horizontal
320 wind speed is about 2 m s^{-1} on Dec. 23, 2013. On Dec. 02, 2013 (“transition”), the basin is
321 influenced by the trough in the north and the high in the south on 850 hPa, and the variation
322 of meteorological conditions inside the basin are determined by the development of the
323 trough and the high. From the early morning to the noontime, the airflow inside the basin

varies from convergence to divergence and the wind gets stronger, indicating the deepening of the trough in the north and the possible evacuation of pollutants from the basin. In general, the synoptic pattern influencing the basin experience the transition from "inland-high" to "southwest-trough", so the pollutants accumulated in the basin in the morning have potentials to be transported outside of the basin in the afternoon/evening, depending on the deepening of the trough in the north on 850 hPa.

Figure 8 presents the observed and simulated spatial distributions of near-surface $PM_{2.5}$ mass concentrations along with the modeled wind fields in the Guanzhong basin at 09:00 and 15:00 BJT on the selected 6 days. The calculated patterns of $PM_{2.5}$ mass concentrations are generally consistent with the observation over the ambient monitoring sites on those days. Under the favorable situations, the strong north or northwest winds have commenced to evacuate the air pollutants accumulated during nighttime at 09:00 BJT (Figures 8b and 8c), and the whole basin becomes clean at 15:00 BJT. In case of unfavorable situations, the near-surface winds in the basin are weak or calm and frequently disordered, which facilitates the accumulation of air pollutants, causing heavy air pollution. The modeled and observed $PM_{2.5}$ mass concentrations exceed 150 $\mu g\ m^{-3}$ at most of monitoring sites. Particularly, on Dec. 23, 2013 ("inland-high"), the basin experienced severe air pollution with the $PM_{2.5}$ mass concentrations exceeding 250 or even 500 $\mu g\ m^{-3}$ at monitoring sites. On Jan. 23, 2014 ("southeast-trough"), the near-surface south winds over Qinling Mountains are not weak, but, apparently, the warm and humid air from the south does not significantly influence the wind fields in the basin. Unfortunately, the south winds over the Qinling Mountains carry the warm air aloft the basin, causing the temperature inversion and further hindering the diffusion of air pollutants in the vertical direction (Figure 6e). So in the condition of "southeast-trough", the whole basin seems to be sealed and is often severely polluted, i.e., the 5-year average filter measured $PM_{2.5}$ mass concentration exceeds 300 $\mu g\ m^{-3}$ at the IEECAS

site (Figure 5). Figure 9 provides the comparison of observed and predicted diurnal profiles of the $PM_{2.5}$ mass concentrations averaged over the monitoring sites in the Guanzhong basin on the selected six days. The WRF-CHEM model generally captures well the observed diurnal variations of the $PM_{2.5}$ mass concentrations, but it often underestimates the observation in the early morning and overestimates during rush hours. Under favorable synoptic situations, the average $PM_{2.5}$ mass concentrations over monitoring sites are significantly decreased from the early morning to the late afternoon, and the air quality can reach the good level during daytime. However, in the conditions of unfavorable synoptic situations, the average $PM_{2.5}$ mass concentrations are less decreased or even increased in the afternoon when the PBL well develops. The unfavorable synoptic situations generally induce the stagnant circumstances, retaining the air pollutants inside the basin. In the afternoon with the peak of sunlight, the elevated air pollutants, including the precursors of secondary aerosols, cause the rapid formation of secondary aerosols, such as nitrate and SOA, compensating the decrease of $PM_{2.5}$ mass concentrations due to the development of the PBL. Furthermore, high levels of aerosols in the low-level atmosphere also scatter the solar radiation and reduce the surface temperature, suppressing the development of the PBL. So the formation of secondary aerosols and the aerosol radiation feedback likely lead to the high level $PM_{2.5}$ mass concentration in the afternoon in case of unfavorable synoptic situations. Figure 10 displays a scatterplot of the measured versus modeled daily mean mass concentration of major aerosol constituents at IEECAS site on the selected six days. The filter measured organic carbon is scaled by a factor of 1.8 to compare with the simulated organic aerosol (Carlton et al., 2010). The WRF-CHEM model performs reasonably in simulating daily mean sulfate, ammonium, organic aerosols and elemental carbon. However, the model consistently overestimates the observed ammonium aerosol mass concentration. The filter measurements show that the $PM_{2.5}$ in the basin contains abundant potassium, sodium, and

374 calcium ions which are originated from biomass burning or dust and able to preferentially
375 replace the ammonium ions. In the WRF-CHEM simulations, the contributions of potassium,
376 sodium, and calcium ions are not considered due to lack of available emissions inventories,
377 so when the ammonia is sufficient in the atmosphere, the overestimation of ammonium
378 aerosols can be explained. In general, the simulated $PM_{2.5}$ patterns and variations on the
379 selected six days are well consistent with the corresponding synoptic situations.
380

381 **4. Conclusions and Discussions**

382 In the present study, the typical synoptic situations influencing the Guanzhong basin
383 during wintertime have been investigated to evaluate their potential impacts on the air quality
384 in the basin through using NCEP reanalysis data, aerosol measurements, and simulations by
385 the FLEXPART, WRF and WRF-CHEM models. The results show that the synoptic
386 situations significantly contribute to the air pollution in the basin during wintertime.

387 Based on the NCEP reanalysis data, the large-scale synoptic situations influencing the
388 Guanzhong basin during the wintertime of 2013 are categorized into six types, including
389 "north-low", "southwest-trough", "southeast-high", "transition", "southeast-trough", and
390 "inland-high". The FLEXPART trajectory model has been utilized to examine the
391 corresponding pollutant transport patterns for the typical synoptic situations in the basin. The
392 pollutants are transported outside of the basin in case of "southwest-trough" and "southeast-
393 high", which are defined as favorable synoptic situations. The rest four types of synoptic
394 conditions, defined as unfavorable synoptic situations, are subject to pollutant accumulation
395 in the basin, causing heavy air pollution. In association with the $PM_{2.5}$ measurements released
396 by the China MEP, the favorable synoptic situations efficiently decrease $PM_{2.5}$ mass
397 concentrations or significantly improve the air quality in the basin and vice versa.

398 The analysis of the large-scale synoptic situations of the wintertime during 2008 to

2012 shows that unfavorable synoptic situations constitute about 85% of the winter days, indicating the significant contribution from the large-scale meteorological conditions to the poor air quality in the Guanzhong basin. In addition, the percentage of "inland-high" is around 42%, which is the most popular synoptic situation associated with the poor air quality in the basin.

The WRF-CHEM model has been further used to simulate the selected six days representing the typical synoptic situations during the wintertime of 2013, and the results shows that the modeled $PM_{2.5}$ distribution and variations are generally consistent well with the corresponding synoptic conditions, which demonstrates the critical role of the synoptic meteorological conditions in air pollution events in the basin. The WRF-CHEM model simulations also indicate the reasonable classification for the synoptic situations in the basin. In addition, detailed meteorological conditions, including temperature inversion, low-level horizontal wind speed, vertical wind velocity, and convergence are also analyzed for the selected days. Under unfavorable synoptic situations, temperature inversion, weak low-level wind and convergence do not facilitate the dispersion of pollutants in the basin. While in the favorable synoptic situations, low-level divergence, caused by strong horizontal winds or active vertical motions, efficiently evacuate air pollutants in the basin.

During wintertime, 5-year filter $PM_{2.5}$ measurement from 2008 to 2012 and the $PM_{2.5}$ measurement released by China MEP in 2013 and 2014 all show that the Guanzhong basin has experienced heavy air pollution. Even under favorable synoptic situations, the observed $PM_{2.5}$ mass concentrations have barely reached the excellent level due to massive local emissions of air pollutants and the background dust transportation from Loess Plateau. Hence, considering the proportion of occurrence of unfavorable synoptic situations during wintertime, reduction of emissions is a feasible method to reduce the air pollution in the Guanzhong basin.

Given that the synoptic situations categorized are made at 850 hPa that influence the Guanzhong basin, potential uncertainties still exist in the classification results. More quantitative studies are needed in the future to improve the synoptic situation classification. Further, the analysis using local meteorological observations on ground surfaces and inside the PBL is also imperative to investigate the role of the local meteorological conditions in the severe pollution events.

Acknowledgement

Naifang Bei is supported by the National Natural Science Foundation of China (no. 41275101) and the Fundamental Research Funds for the Central Universities of China. Guohui Li is supported by "Hundred Talents Program" of the Chinese Academy of Sciences and the National Natural Science Foundation of China (no. 41275153).

References

Bei, N., Lei, W., Zavala, M., and Molina, L. T.: Ozone predictabilities due to meteorological uncertainties in Mexico City Basin using ensemble forecasts, Atmos. Chem. Phys., 10, 6295–6309, 2010.

Bei, N., de Foy, B., W., Zavala, M., and Molina, L. T: Using 3DVAR data assimilation system to improve ozone simulations in the Mexico City basin, Atmos. Chem. Phys., 8, 7353-7366, 2008.

Bei, N., Li, G., and Molina, L. T.: Uncertainties in SOA simulations due to meteorological uncertainties in Mexico City during MILAGRO-2006 field campaign, Atmos. Chem. Phys., 12, 11295-11308, doi:10.5194/acp-12-11295-2012, 2012.

Bei, N., Li, G., Zavala, M., et al.: Meteorological overview and plume transport patterns during Cal-Mex 2010, Atmos. Environ., 70, 477-489, 2013.

Binkowski, F. S., and Roselle, S. J.: Models-3 Community Multiscale Air Quality (CMAQ) model aerosol component: 1. Model description, Journal of Geophysical Research, J. Geophys. Res., 4183, doi:10.1029/2001JD001409, 2003.

Cao, J.J., Zhu, C.S., Chow, J.C., et al.: Black carbon relationships with emissions and meteorology in Xi'an, China, Atmos. Res., 94, 194–202, 2009.

Cao, J.J., Wang, Q.Y., Chow, J.C., et al.: Impacts of aerosol compositions on visibility impairment in Xi'an, China, Atmos. Environ., 59, 559–566, 2012.

Chan, C. K., and Yao, X.: Air pollution in mega cities in China, Atmos. Environ., 42, 1–42, 2008.

Chen, Z., Cheng, S., Li, J., Guo, X., Wang, W., and Chen, D.: Relationship between atmospheric pollution processes and synoptic pressure patterns in Northern China, Atmos. Environ., 42, 6078– 6087, 2008.

Cheng, W. L., Pai, J. L., Tsuang, B. J., and Chen, C. L.: Synoptic patterns in relation to ozone concentrations in West-Central Taiwan, Meteorol. Atmos. Phys., 78, 11–21, 2001.

de Foy, B., Caetano, E., Magan˜a, V., Zita´cuaro, A., Ca´rdenas, B., Retama, A., Ramos, R., Molina, L. T., and Molina, M. J.: Mexico City basin wind circulation during the MCMA-2003 field campaign, Atmos. Chem. Phys., 5, 2267–2288, 2005.

de Foy, B., Varela, J. R., Molina, L. T., and Molina, M. J.: Rapid ventilation of the Mexico City basin and regional fate of the urban plume, Atmos. Chem. Phys., 6, 2321–2335, 2006.

Fang, M., Chan, C. K., and Yao, X. H.: Managing air quality in a rapidly developing nation: China, Atmos. Environ., 43, 79–86, 2009.

Fast, J., and Easter, R.: A Lagrangian Particle Dispersion Model Compatible with WRF, 2006. 7th WRF Users Workshop, NCAR, 19-22 June, Boulder, Colorado, 2006.

Fu, G. Q., Xu, W. Y., Yang, R. F., Li, J. B., and Zhao, C. S.: The distribution and trends of fog and haze in the North China Plain over the past 30 years, Atmos. Chem. Phys., 14, 11949–11958, doi:10.5194/acp-14-11949-2014, 2014.

Gao, Y., Liu, X., Zhao, C., and Zhang, M.: Emission controls versus meteorological conditions in determining aerosol concentrations in Beijing during the 2008 Olympic Games, Atmos. Chem. Phys., 11, 12437–12451, doi:10.5194/acp-11-12437-2011, 2011.

Grell, G. A., Devenyi, D.: A generalized approach to parameterizing convection combining

ensemble and data assimilation techniques, Geophys. Res. Lett., 29 (14), doi:10.1029/2002GL015311, 2002.

Grell, G. A., Peckham, S. E., Schmitz, R., McKeen, S. A., Wilczak, J., and Eder, B.: Fully coupled "online" chemistry within the WRF model, Atmos. Environ., 39, 6957–6975, 2005.

Guenther, A., Karl, T., Harley, P., Wiedinmyer, C., Palmer, P. I., and Geron, C.: Estimates of global terrestrial isoprene emissions using MEGAN (Model of Emissions of Gases and Aerosols from Nature), Atmos. Chem. Phys., 6, 3181–3210, doi:10.5194/acp-6-3181-2006, 2006.

Guo, S., M. Hu, M. L. Zamora, J. Peng, D. Shang, J. Zheng, Z. Du, Z. Wu, M. Shao, L. Zeng, M. J. Molina, and R. Zhang: Elucidating severe urban haze formation in China, Proc Natl Acad Sci USA, 111, 17373-17378, 2014.

Han, S., Wu, J., Zhang, Y., Cai, Z., Feng, Y., Yao, Q., Li, X., Liu, Y., Zhang, M., Characteristics and formation mechanism of a winter hazeefog episode in Tianjin, China, Atmos. Environ., 98, 323-330, 2014.

Hong, S.-Y., Dudhia, J., and Chen, S.-H.: A revised approach to ice microphysical processes for the bulk parameterization of clouds and precipitation, Mon. Wea. Rev., 132, 103–120, 2004.

Huang, R. J., Zhang, Y. L., Bozzetti, C., Ho, K. F., Cao, J. J., Han, Y. M., Dällenbach, K. R., Slowik, J. G., Platt, S. M., Canonaco, F., Zotter, P., Wolf, R., Pieber, S. M., Bruns, E. A., Crippa, M., Ciarelli, G., Piazzalunga, A., Schwikowski, M., Abbaszade, G., Schnelle-Kreis, J., Zimmermann, R., An, Z. S., Szidat, S., Baltensperger, U., EI Haddad, I., Prévôt, A. S. H.: High secondary aerosol contribution to particulate pollution during haze events in China. Nature, 514, 218-222, 2014.

Huang, K., Zhuang, G., Lin, Y., Fu, J. S., Wang, Q., Liu, T., Zhang, R., Jiang, Y., Deng, C., Fu, Q., Hsu, N. C., and Cao, B.: Typical types and formation mechanisms of haze in an Eastern Asia megacity, Shanghai, Atmos. Chem. Phys., 12, 105–124, 2012.

Huth, R., Beck, C., Philipp, A., Demuzere, M., Ustrnul, Z., Cahynová, M., Kysely´, J., and Tveito, O. E.: Classifications of atmospheric circulation patterns, Ann. NY Acad. Sci., 1146, 105–152, 2008.

Jacobeit, J.: Classifications in climate research, Phys. Chem. Earth, 35, 411–421, 2010.

Janjic, Z. I.: Nonsingular implementation of the Mellor-Yamada level 2.5 scheme in the NCEP Meso Model, NCEP Office Note, 437, 61 pp., 2002.

Li, G., Bei, N., Tie, X., and Molina, L. T.: Aerosol effects on the photochemistry in Mexico City during MCMA-2006/MILAGRO campaign, Atmos. Chem. Phys., 11, 5169-5182, 2011a.

Li, G., Zavala, M., Lei, W., Tsimpidi, A. P., Karydis, V. A., Pandis, S. N., Canagaratna, M. R., and Molina, L. T.: Simulations of organic aerosol concentrations in Mexico City using the WRF-CHEM model during the MCMA-2006/MILAGRO campaign, Atmos. Chem. Phys., 11, 3789-3809, 2011b.

Li, G., Lei, W., Zavala, M., Volkamer, R., Dusanter, S., Stevens, P., and Molina, L. T.: Impacts of HONO sources on the photochemistry in Mexico City during the MCMA-2006/MILAGRO Campaign, Atmos. Chem. Phys., 10, 6551–6567, 2010.

525 Li, G., Lei, W., Bei, N., and Molina, L. T.: Contribution of garbage burning to chloride and
526 $PM_{2.5}$ in Mexico City, Atmos. Chem. Phys., 12, 8751-8761, doi:10.5194/acp-12-8751-
527 2012, 2012.

528 Liu, X., Li, J., Qu, Y., Han, T., Hou, L., Gu, J., Chen, C., Yang, Y., Yang, T., Zhang, Y.,
529 Tian, H.Z., Hu, M.: Formation and evolution mechanism of regional haze: a case study in
530 the megacity Beijing, China. Atmos. Chem. Phys. 13, 4501–4514, 2013.

531 Penner, J. P., et al.: Aerosols, their direct and indirect effects. In: Houghton, J.T., et al. (Eds.),
532 Climate Change 2001: The Scientific Basis. Contribution of Working Group I to the Third
533 Assessment Report of the Intergovernmental Panel on Climate Change. Cambridge
534 University Press, Cambridge, pp. 289–348, 2001.

535 Philipp, A., Bartholy, J., Beck, C., Erpicum, M., Esteban, P., Fettweis, X., Huth, R., James, P.,
536 Jourdain, S., and Kreienkamp, F.: COST733CAT-a database of weather and circulation
537 type classifications, Phys. Chem. Earth, 35, 360–373, 2010.

538 Pope Iii, C. A. and Dockery, D. W.: Health effects of fine particulate air pollution: lines that
539 connect, J. Air Waste Manage., 56, 709– 742, 2006.

540 Seaman, N. L.: Meteorological modeling for air-quality assessments, Atmos. Environ., 34,
541 2231–2259, 2000.

542 Shen, Z. X., Cao, J. J., Arimoto, R., et al.: Chemical characteristics of fine particles (PM1)
543 over Xi'an, China, Aerosol Sci. Tech., 44, 461–472, 2010.

544 Shen, Z. X., Cao, J. J., Liu, S. X., et al.: Chemical composition of PM10 and $PM_{2.5}$ collected
545 at ground level and 100-m during a strong winter-time pollution episode in Xi'an, China, J.
546 Air Waste Manage., 61, 11, 1150–1159, 2011.

547 Skamarock, W. C., Klemp, J. B., Dudhia, J., Gill, D. O., Barker, D. M., Duda, M., Huang, X.-
548 Y., Wang, W., Powers, J. G.: A Description of the Advanced Research WRF Version 3,
549 NCAR Technical Note, Boulder, CO., 2008.

550 Solomon, P., Cowling, E., Hidy, G., and Furiness, C.: Comparison of scientific findings from
551 major ozone field studies in North America and Europe, Atmos. Environ., 34, 1885–1920,
552 2000.

553 Stohl, A., Hittenberger, M., Wotawa, G.: Lagrangian particle dispersion model FLEXPART
554 against large scale tracer experiment data. Atmos. Environ., 32, 4245-4264, 1998.

555 Wang, H., Xu, J., Zhang, M., Yang, Y., Shen, X., Wang, Y., Chen, D., Guo, J.: A study of the
556 meteorological causes of a prolonged and severe haze episode in January 2013 over
557 central-eastern China, Atmos. Environ., 98, 146-157, 2014a.

558 Wang, L., N. Zhang, Z. Liu, Y. Sun, D. Ji, and Y. Wang: The Influence of Climate Factors,
559 Meteorological Conditions, and Boundary-Layer Structure on Severe Haze Pollution in
560 the Beijing-Tianjin-Hebei Region during January 2013, Adv. Meteorol., 2014, 1-14,
561 2014b.

562 Wang, Y., Hao, J., McElroy, M. B., Munger, J. W., Ma, H., Chen, D., and Nielsen, C. P.:
563 Ozone air quality during the 2008 Beijing Olympics: effectiveness of emission restrictions,
564 Atmos. Chem. Phys., 9, 5237–5251, doi:10.5194/acp-9-5237-2009, 2009.

565 Wei, P., Cheng, S., Li, J., and Su, F.: Impact of boundary-layer anticyclonic weather system
566 on regional air quality, Atmos. Environ., 45, 2453–2463, 2011.

567 Wu, D., G. Liao, X. Deng, X. Bi, H. Tan, F. Li, C. Jiang, D. Xia, and S. Fan, Transport

Condition of Surface Layer Under Haze Weather over the Pearl River Delta, J. Appl. Meteor. Sci. (in Chinese), 19, 1-9, 2008.

Wu, M., Wu, D., Fan, Q., Wang, B. M., Li, H. W., and Fan, S. J.: Observational studies of the meteorological characteristics associated with poor air quality over the Pearl River Delta in China, Atmos. Chem. Phys., 13, 10755–10766, doi:10.5194/acp-13-10755-2013, 2013.

Yang, Y., Liu, X., Qu, Y., Wang, J., An, J., Zhang, Y., Zhang, F.: Formation mechanism of continuous extreme haze episodes in the megacity Beijing, China, in January 2013, Atmos. Res., 155, 192–203, 2015.

Zhang, J., Mauzerall, D. L., Zhu, T., Liang, S., Ezzati, M., and Remais, J. V.: Environmental health in China: progress towards clean air and safe water, The Lancet, 375, 1110–1119, 2010.

Zhang, J. P., Zhu, T., Zhang, Q. H., Li, C. C., Shu, H. L., Ying, Y., Dai, Z. P., Wang, X., Liu, X. Y., Liang, A. M., Shen, H. X., and Yi, B. Q.: Impact of circulation patterns on transport paths and air quality, Atmos. Chem. Phys., 12, 5031–5053, 2012.

Zhang, Q., Streets, D. G., Carmichael, G. R., He, K. B., Huo, H., Kannari, A., Klimont, Z., Park, I. S., Reddy, S., Fu, J. S., Chen, D., Duan, L., Lei, Y., Wang, L. T., and Yao, Z. L.: Asian emissions in 2006 for the NASA INTEX-B mission, Atmos. Chem. Phys., 9, 5131–5153, 2009.

Zhang, Q. H., Zhang, J. P., and Xue, H. W.: The challenge of improving visibility in Beijing, Atmos. Chem. Phys., 10, 7821– 7827, doi:10.5194/acp-10-7821-2010, 2010.

Zhang Q., Quan, J., Tie, X., Li, X., Liu, Q., Gao, Y., and Zhao, D.: Effects of meteorology and secondary particle formation on visibility during heavy haze events in Beijing, China, Sci. Total Environ., 502, 578-584, 2015.

Zhao, X. J., Zhao, P. S., Xu, J., Meng, W., Pu, W. W., Dong, F., He, D., and Shi, Q. F.: Analysis of a winter regional haze event and its formation mechanism in the North China Plain, Atmos. Chem. Phys., 13, 5685–5696, 2013.

598 **Figure Captions**

599 Figure 1. (a) WRF and WRF-CHEM model simulation domain with topography and (b)
600 geographic distributions of ambient monitoring stations. In (b), the blue filled
601 squares are the ambient monitoring sites and the red filled circle is the IEECAS
602 site.

603 Figure 2. Distributions of winds and geopotential heights on 850 hPa at 08:00 BJT on (a) Feb.
604 16, 2014 ("north-low"), (b) Jan. 19, 2014 ("southwest-trough"), (c) Dec. 26, 2013
605 ("southeast-high"), (d) Dec. 2, 2013 ("transition"), (e) Jan. 23, 2014 ("southeast-
606 trough"), and (f) Dec. 23, 2013 ("inland-high"). The red filled circle is Xi'an.

607 Figure 3. 24-hour plume transport patterns initialized from 04:00 BJT on (a) Feb. 16, 2014
608 ("north-low"), (b) Jan. 19, 2014 ("southwest-trough"), (c) Dec. 26, 2013
609 ("southeast-high"), (d) Dec. 2, 2013 ("transition"), (e) Jan. 23, 2014 ("southeast-
610 trough"), and (f) Dec. 23, 2013 ("inland-high").

611 Figure 4. Diurnal cycle of observed $PM_{2.5}$ mass concentrations averaged over 33 monitoring
612 sites in the Guanzhong basin under the six synoptic categories during the
613 wintertime of 2013.

614 Figure 5. Daily mean $PM_{2.5}$ mass concentration averaged during the six typical synoptic
615 situations from 2008 to 2012 at the IEECAS site.

616 Figure 6. Vertical distributions of temperature, wind vectors, and PBL height through Xi'An
617 along the east-west direction at 09:00 and 15:00 BJT on (a) Feb. 16, 2014 ("north-
618 low"), (b) Jan. 19, 2014 ("southwest-trough"), (c) Dec. 26, 2013 ("southeast-
619 high"), (d) Dec. 2, 2013 ("transition"), (e) Jan. 23, 2014 ("southeast-trough"), and
620 (f) Dec. 23, 2013 ("inland-high"). The black filled rectangle represents the urban
621 area of Xi'an, China.

622 Figure 7. Temporal variations of the area averaged low-level vertical velocity, divergence,
623 and wind speed over the basin on (a) Feb. 16, 2014 ("north-low"), (b) Jan. 19,
624 2014 ("southwest-trough"), (c) Dec. 26, 2013 ("southeast-high"), (d) Dec. 2, 2013
625 ("transition"), (e) Jan. 23, 2014 ("southeast-trough"), and (f) Dec. 23, 2013
626 ("inland-high").

627 Figure 8. Pattern comparison of simulated vs. observed near-surface $PM_{2.5}$ mass
628 concentrations at 09:00 and 15:00 BJT on (a) Feb. 16, 2014 ("north-low"), (b) Jan.
629 19, 2014 ("southwest-trough"), (c) Dec. 26, 2013 ("southeast-high"), (d) Dec. 2,
630 2013 ("transition"), (e) Jan. 23, 2014 ("southeast-trough"), and (f) Dec. 23, 2013
631 ("inland-high"). Colored squares: $PM_{2.5}$ observations; color contour: $PM_{2.5}$
632 simulations; black arrows: simulated surface winds.

633 Figure 9. Comparison of observed and predicted diurnal profiles of the $PM_{2.5}$ mass
634 concentrations averaged over the monitoring sites in the Guanzhong basin on (a)
635 Feb. 16, 2014 ("north-low"), (b) Jan. 19, 2014 ("southwest-trough"), (c) Dec. 26,
636 2013 ("southeast-high"), (d) Dec. 2, 2013 ("transition"), (e) Jan. 23, 2014
637 ("southeast-trough"), and (f) Dec. 23, 2013 ("inland-high").

638 Figure 10. Scatter plot of the measured versus modeled daily mean mass concentration of
639 aerosol constituents at IEECAS site on the selected six days.
640
641
642

643 Table 1 Synoptic categories influencing the Guanzhong basin during the wintertime of 2013
644
645

Categories	Date*	Sum	Percentage (%)
North-low	20131217 20131208 20140110 20140111 20140102 20140106 20140204 20140205 20140206 20140215 20140216 20140217 20140224 20140225 20140228 20140208	16	17.8
Southwest-trough	20131201 20131205 20131209 20131211 20131212 20131215 20131231 20140103 20140104 20140119 20140120 20140108 20140112	13	14.4
Southeast-high	20131210 20131226 20140107 20140227	4	4.4
Transition	20131202 20131207 20131214 20131230 20140101 20140116 20140127 20140130 20140201 20140202 20140207	11	12.2
Southeast-trough	20131204 20140123 20140129 20140131 20140226	5	5.6
Inland-high	20131203 20131206 20131213 20131219 20131221 20131222 20131223 20131224 20131216 20131225 20131218 20131220 20131227 20131229 20131228 20140105 20140113 20140118 20140122 20140125 20140115 20140121 20140126 20140128 20140109 20140114 20140117 20140124 20140214 20140219 20140211 20140210 20140213 20140220 20140221 20140222 20140223 20140218 20140212 20140209 20140203	41	45.6

646
647 *The format of date is YYYYMMDD, in which YYYY, MM, and DD represent year, month, day, respectively.
648
649
650
651

652 Table 2 Days and percentage of the six types of synoptic situations influencing the
653 Guanzhong basin during the wintertime from 2008 to 2012
654

Categories	North low	Southwest trough	Southeast high	Transition	Southeast trough	Inland high
2008	14	8	2	15	11	40
2009	17	6	6	14	18	29
2010	14	10	8	8	6	41
2011	16	6	10	5	3	52
2012	22	9	1	15	13	31
Sum	83	39	27	57	51	193
Percentage (%)	18.4	8.7	6.0	12.7	11.3	42.9

655
656
657
658
659

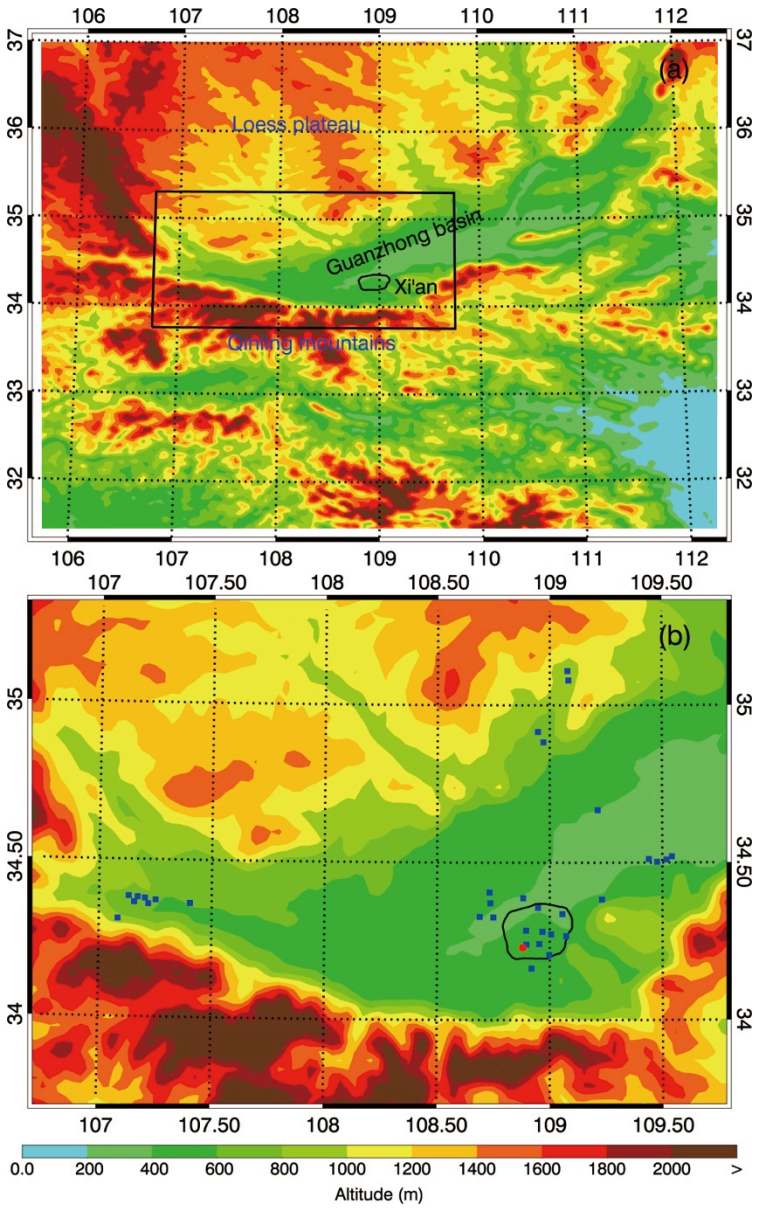
(a)
Loess plateau
Guanzhong basin
Xi'an
Qinling mountains
(b)
106
107
107.50
108
108.50
109
109.50
110
111
112
32
33
34
34.50
35
36
37
0.0
200
400
600
800
1000
1200
1400
1600
1800
2000
>
Altitude (m)

Figure 1

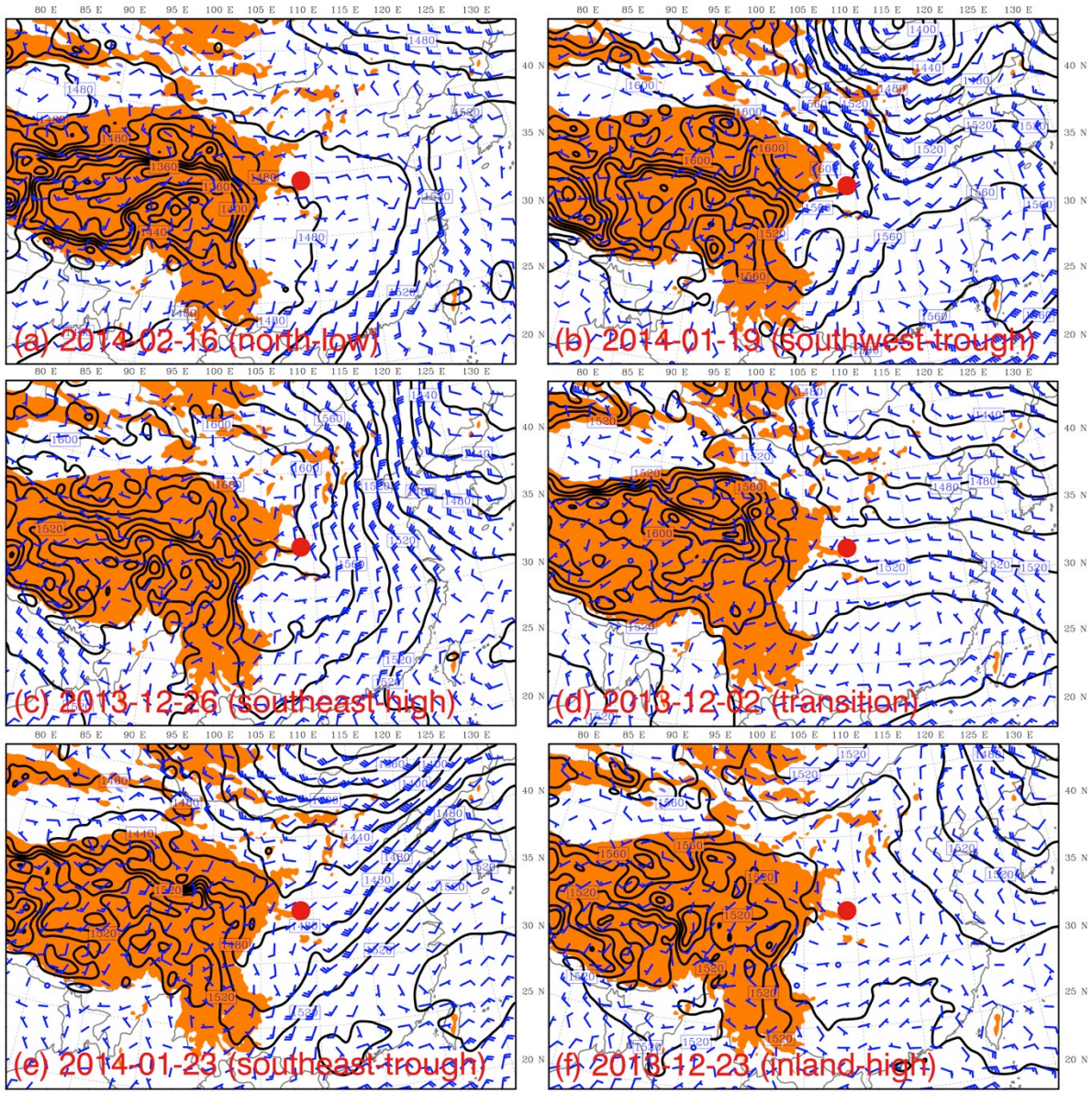
(a) 2014-02-16 (north-low)
(b) 2014-01-19 (southwest-trough)
(c) 2013-12-26 (southeast-high)
(d) 2013-12-02 (transition)
(e) 2014-01-23 (southeast-trough)
(f) 2013-12-23 (inland-high)

Figure 2

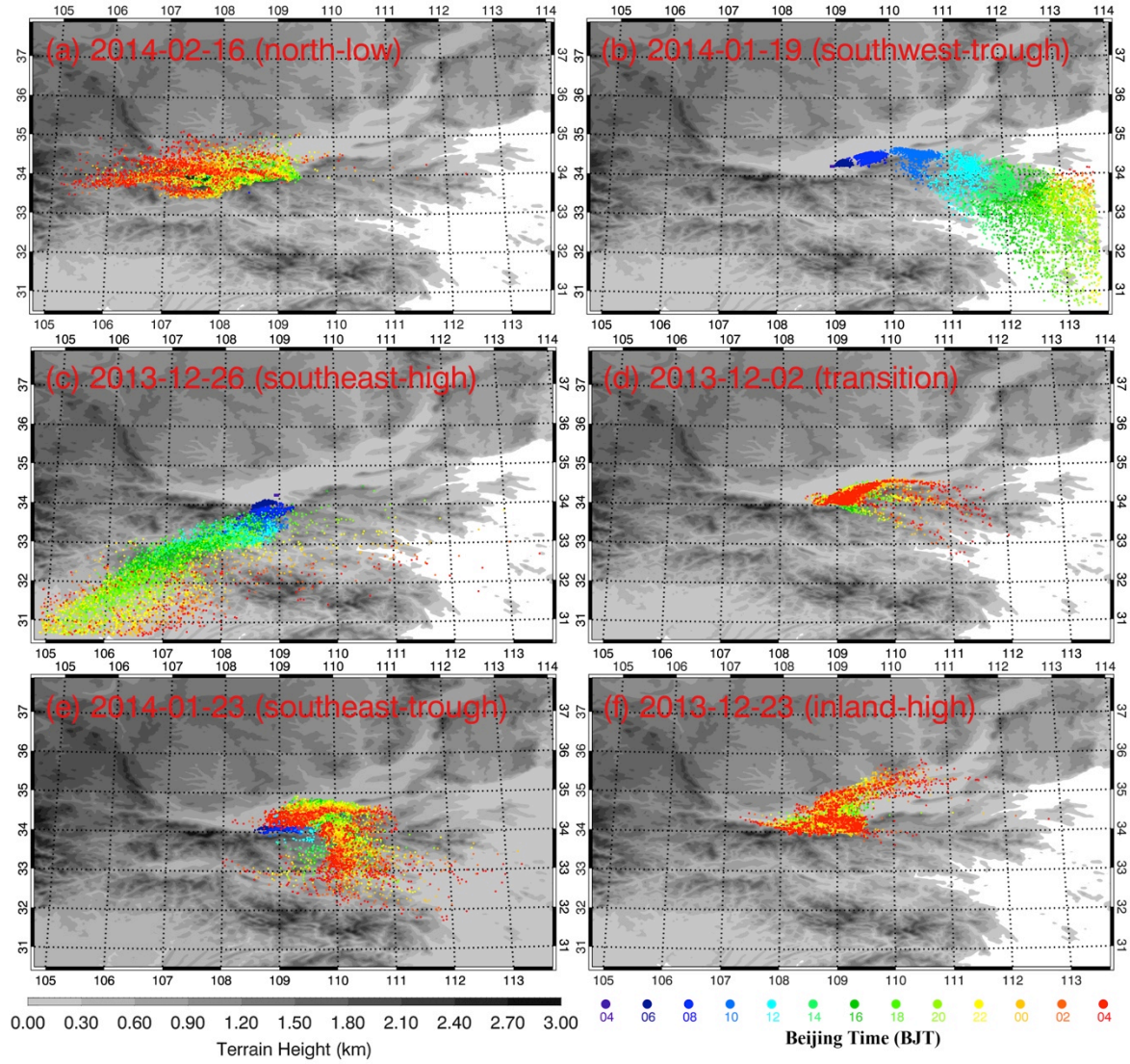
(a) 2014-02-16 (north-low)
(b) 2014-01-19 (southwest-trough)
(c) 2013-12-26 (southeast-high)
(d) 2013-12-02 (transition)
(e) 2014-01-23 (southeast-trough)
(f) 2013-12-23 (inland-high)
0.00 0.30 0.60 0.90 1.20 1.50 1.80 2.10 2.40 2.70 3.00
Terrain Height (km)
04 06 08 10 12 14 16 18 20 22 00 02 04
Beijing Time (BJT)

Figure 3

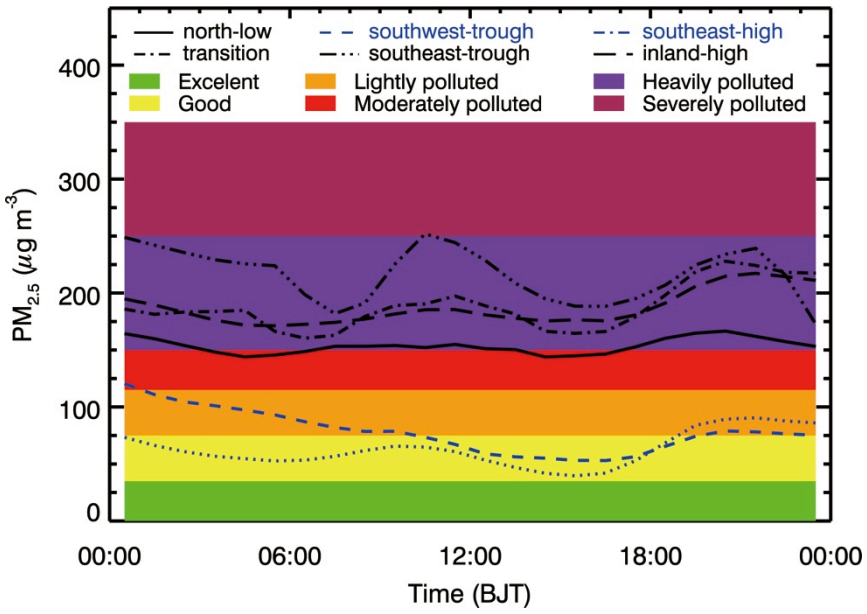
north-low
transition
southwest-trough
southeast-trough
southeast-high
inland-high
Excelent
Good
Lightly polluted
Moderately polluted
Heavily polluted
Severely polluted
400
300
200
100
0
PM2.5 (μg m-3)
00:00
06:00
12:00
18:00
00:00
Time (BJT)

Figure 4

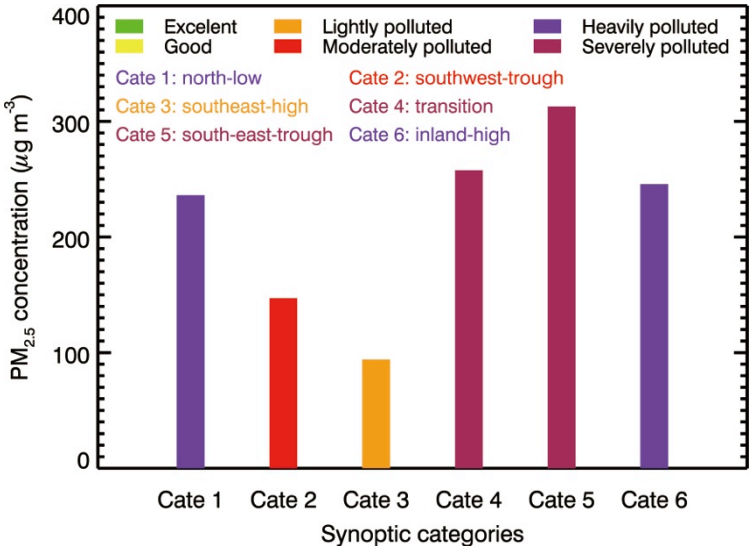
Excelent
Good
Lightly polluted
Moderately polluted
Heavily polluted
Severely polluted
Cate 1: north-low
Cate 2: southwest-trough
Cate 3: southeast-high
Cate 4: transition
Cate 5: south-east-trough
Cate 6: inland-high
PM2.5 concentration (μg m-3)
400
300
200
100
0
Cate 1
Cate 2
Cate 3
Cate 4
Cate 5
Cate 6
Synoptic categories

Figure 5

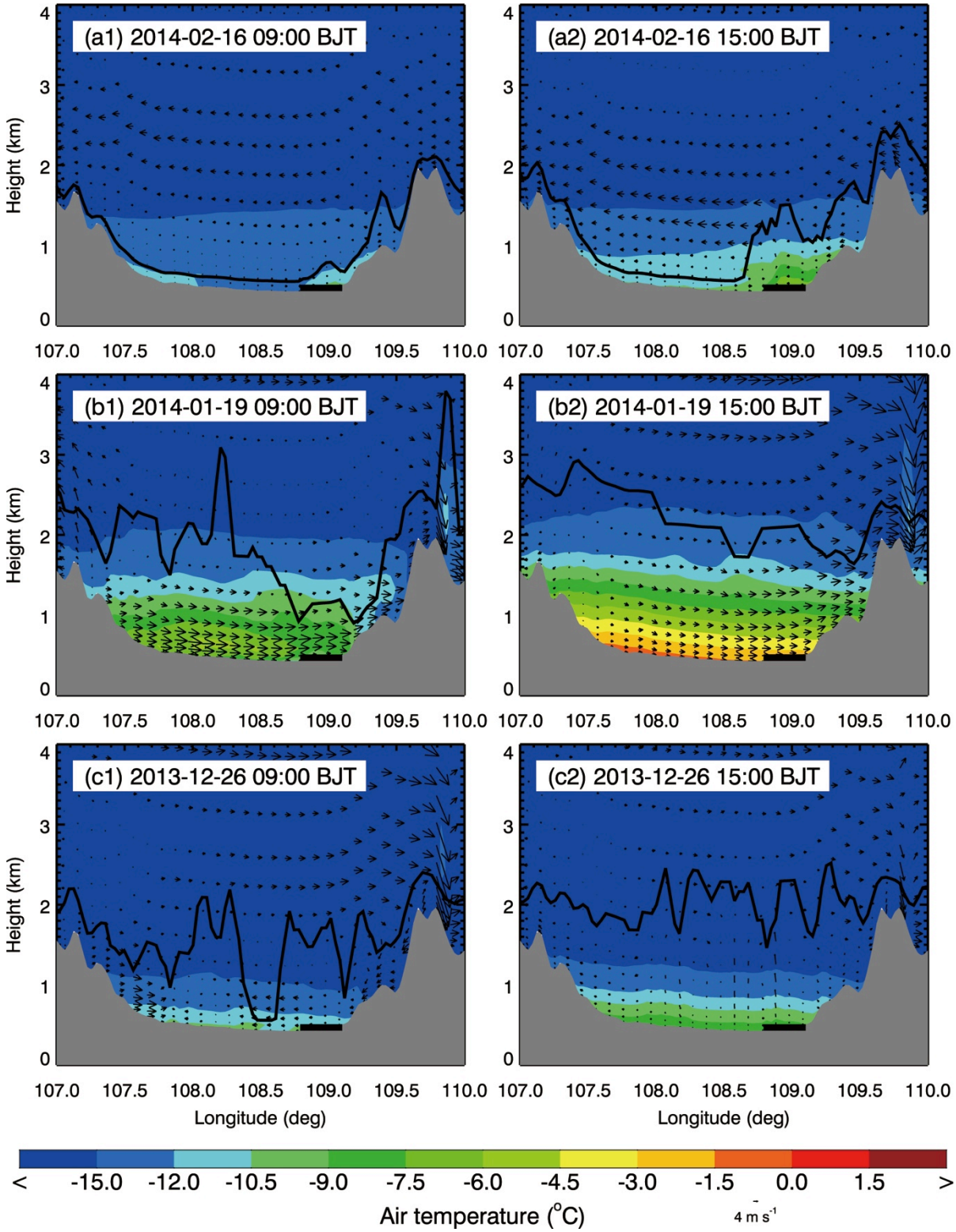
(a1) 2014-02-16 09:00 BJT
(a2) 2014-02-16 15:00 BJT
(b1) 2014-01-19 09:00 BJT
(b2) 2014-01-19 15:00 BJT
(c1) 2013-12-26 09:00 BJT
(c2) 2013-12-26 15:00 BJT
Height (km)
Longitude (deg)
107.0 107.5 108.0 108.5 109.0 109.5 110.0
< -15.0 -12.0 -10.5 -9.0 -7.5 -6.0 -4.5 -3.0 -1.5 0.0 1.5 >
Air temperature (°C)
4 m s-1

Figure 6

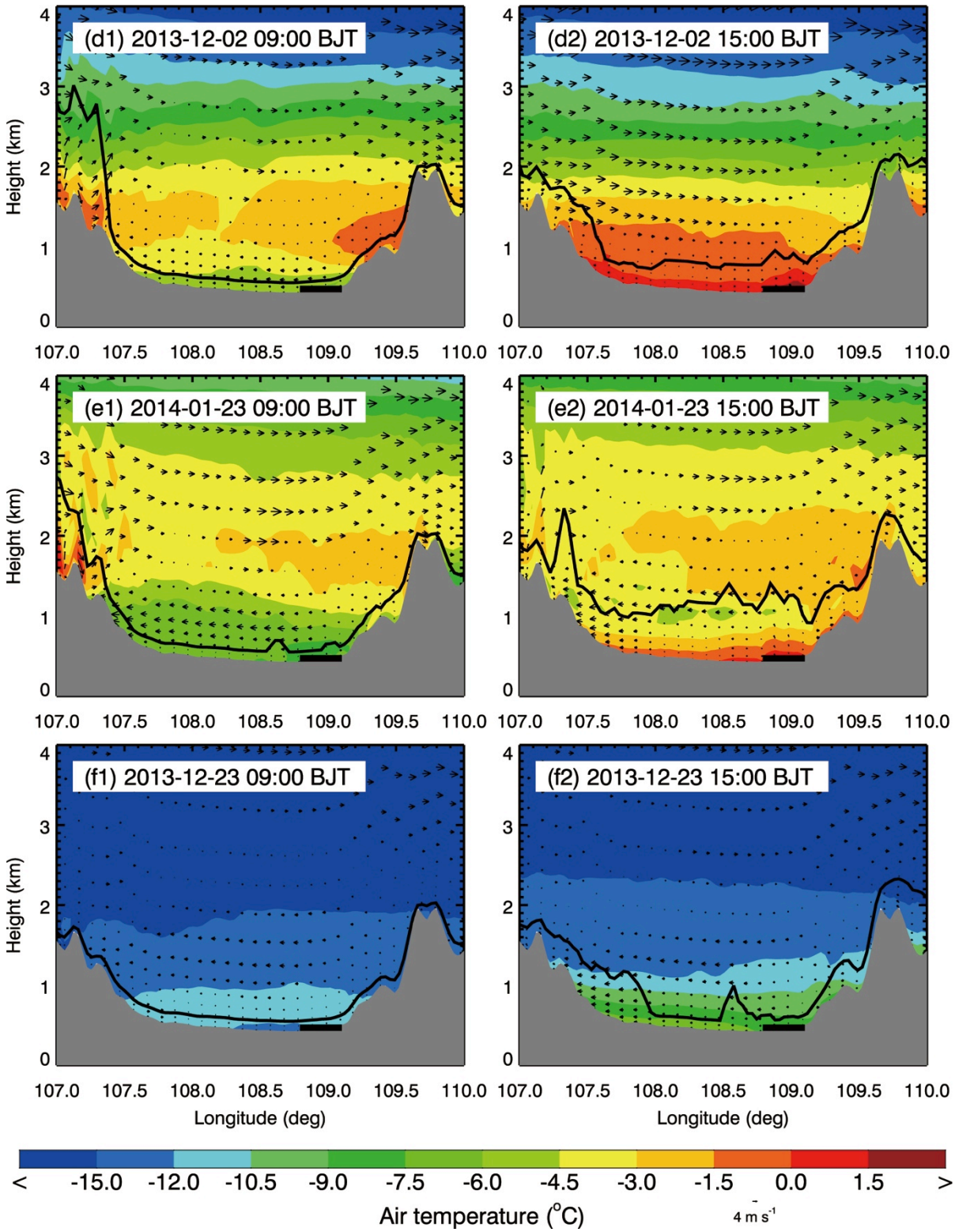

Figure 6 continued

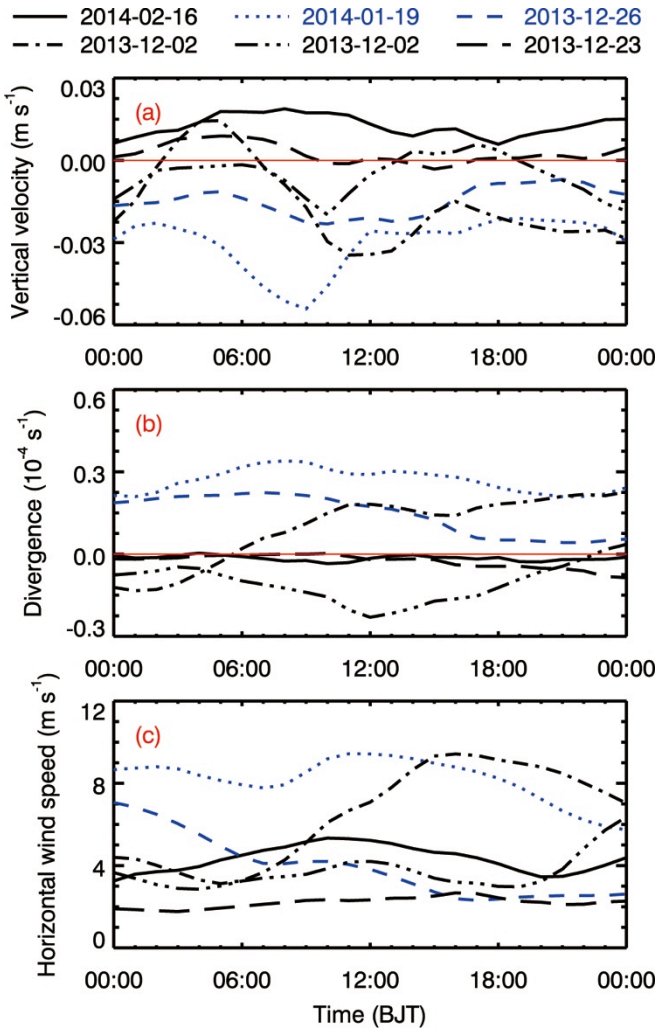
2014-02-16
2014-01-19
2013-12-26
2013-12-02
2013-12-02
2013-12-23
(a)
Vertical velocity (m s-1)
0.03
0.00
-0.03
-0.06
00:00
06:00
12:00
18:00
00:00
(b)
Divergence (10-4 s-1)
0.6
0.3
0.0
-0.3
(c)
Horizontal wind speed (m s-1)
12
8
4
0
Time (BJT)

Figure 7

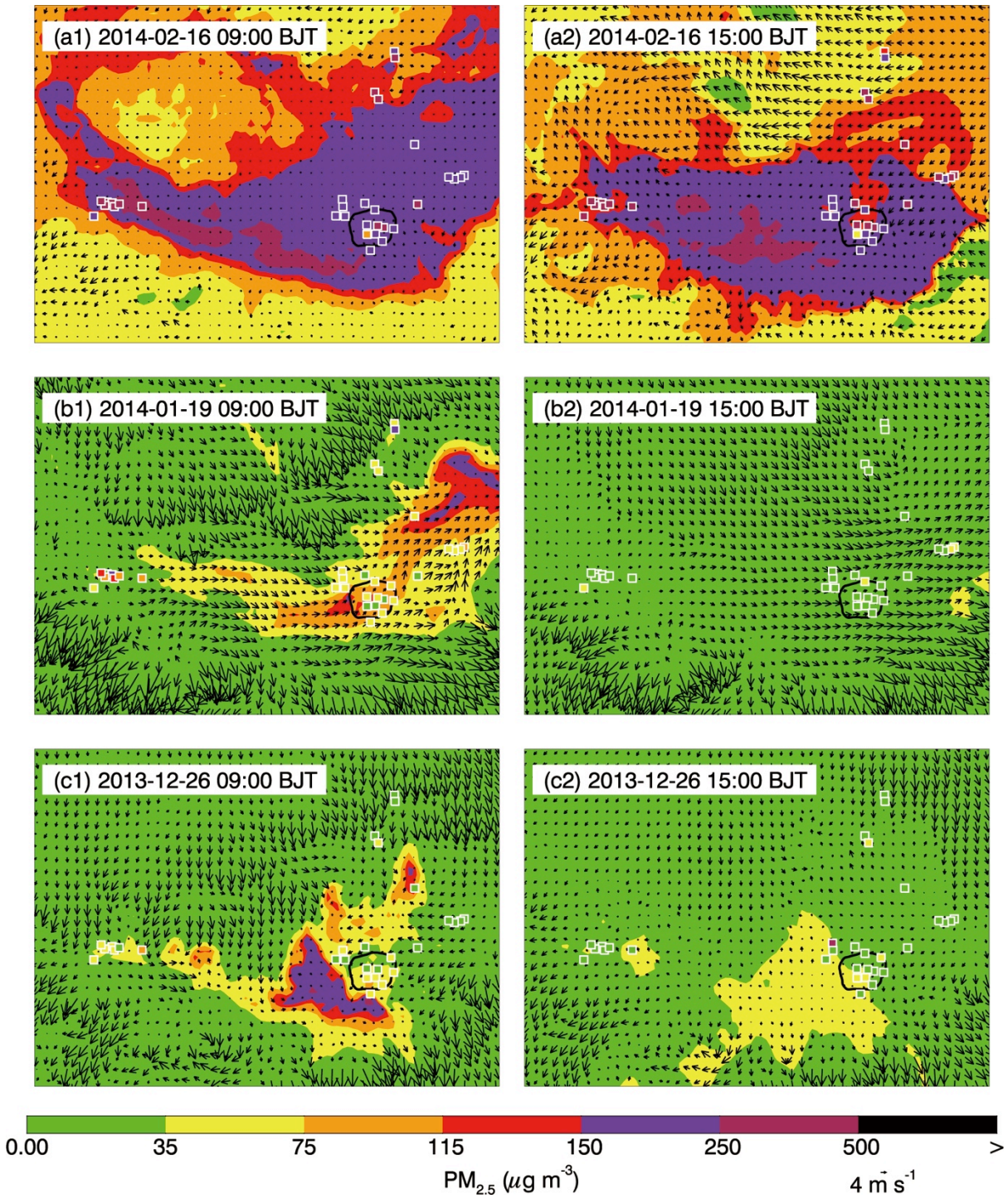
(a1) 2014-02-16 09:00 BJT
(a2) 2014-02-16 15:00 BJT
(b1) 2014-01-19 09:00 BJT
(b2) 2014-01-19 15:00 BJT
(c1) 2013-12-26 09:00 BJT
(c2) 2013-12-26 15:00 BJT
0.00
35
75
115
150
250
500
>
PM2.5 (μg m-3)
4 m s-1

Figure 8

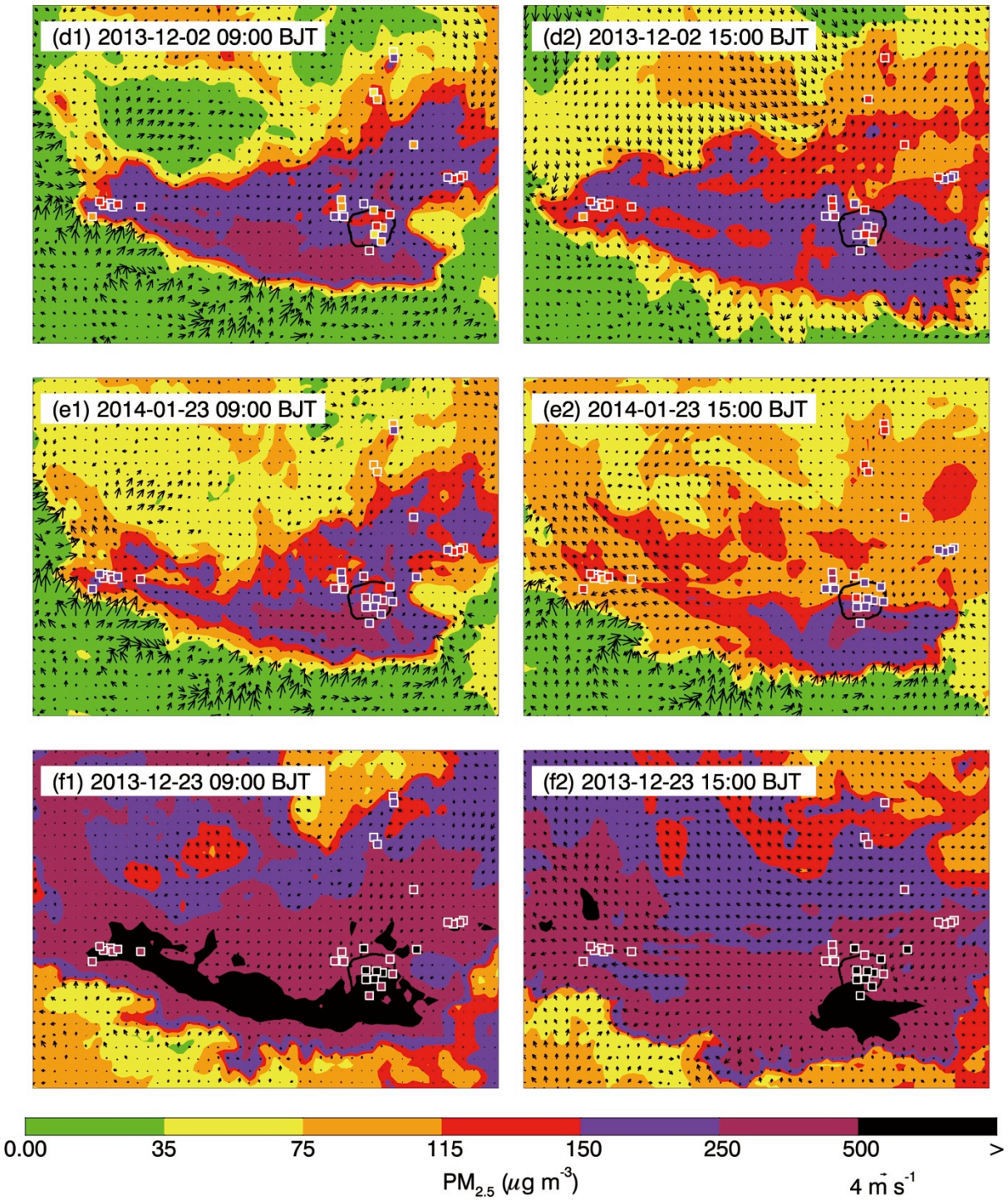

Figure 8 continued

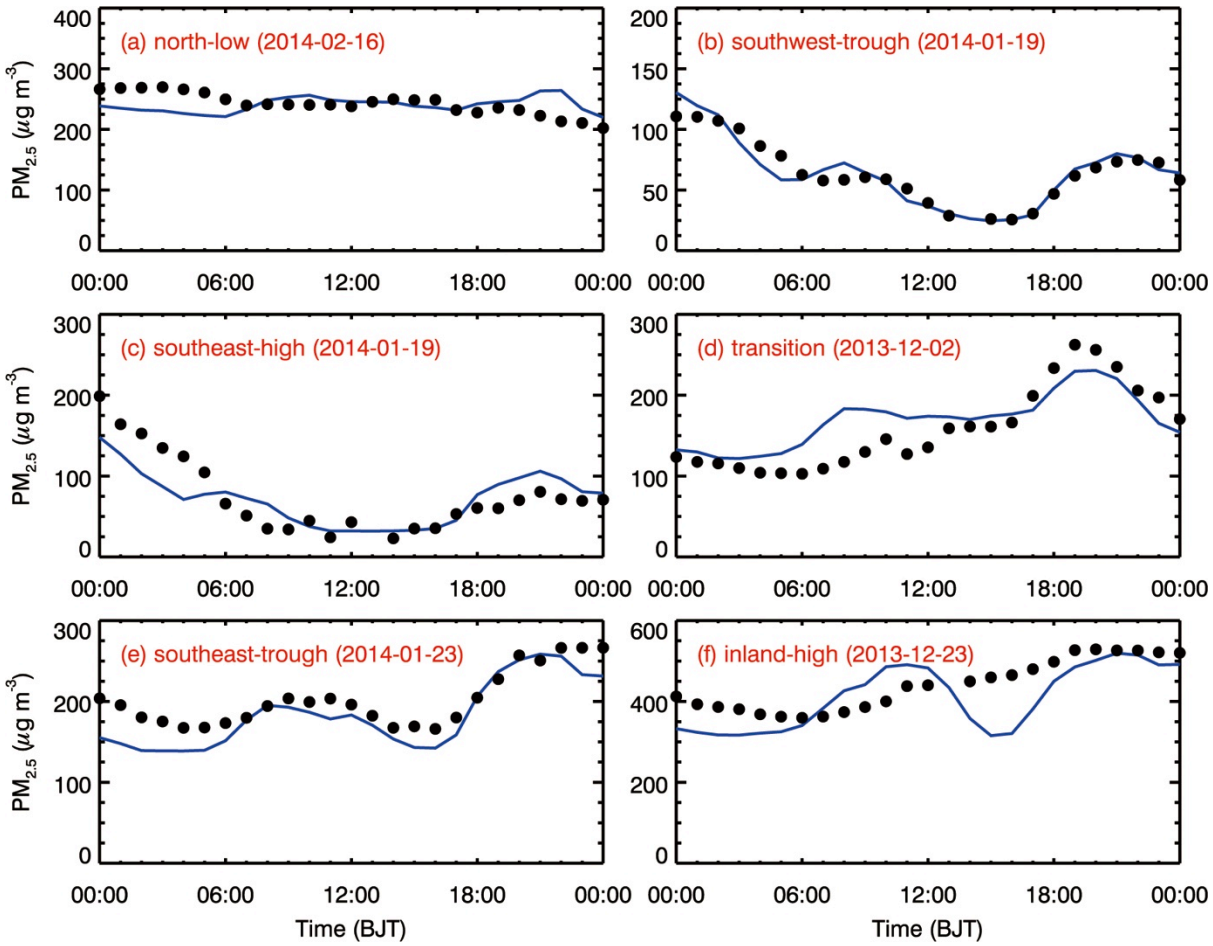
(a) north-low (2014-02-16)
(b) southwest-trough (2014-01-19)
(c) southeast-high (2014-01-19)
(d) transition (2013-12-02)
(e) southeast-trough (2014-01-23)
(f) inland-high (2013-12-23)
PM2.5 (μg m-3)
Time (BJT)
00:00
06:00
12:00
18:00

Figure 9

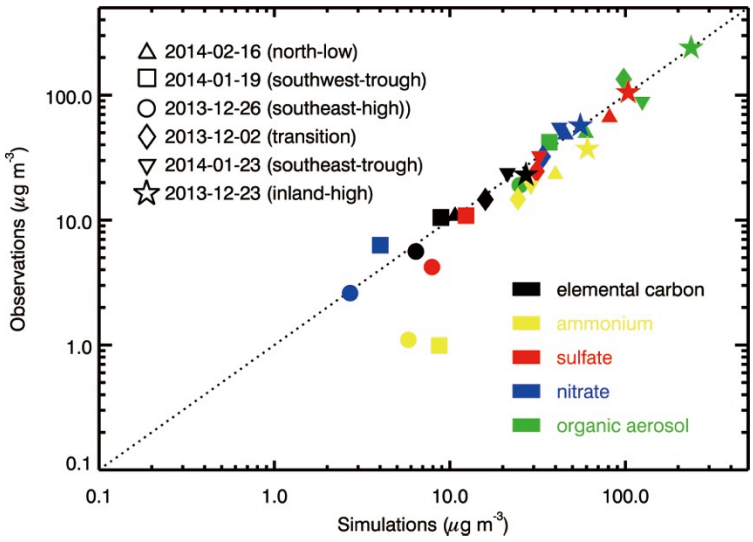

739
740
741 Figure 10